Confirmation of the Stellar Binary Microlensing Event, Macho 97-BLG-28

J. W. Blackman[1,2], J.-P. Beaulieu[1,2], A. A. Cole[1], A. Vandorou[1], N. Koshimoto[3], E. Bachelet[4], V. Batista[2],
A. Bhattacharya[5], and D. P. Bennett[5]

[1] School of Natural Sciences, University of Tasmania, Private Bag 37 Hobart, Tasmania 7001, Australia
[2] Sorbonne Universités, UPMC Université Paris 6 et CNRS, UMR 7095, Institut d'Astrophysique de Paris, 98 bis bd Arago, F-75014 Paris, France
[3] Department of Earth and Space Science, Graduate School of Science, Osaka University, 1-1 Machikaneyama, Toyonaka, Osaka 560-0043, Japan
[4] Las Cumbres Observatory, 6740 Cortona Drive, Suite 102, Goleta, CA 93117, USA
[5] Laboratory for Exoplanets and Stellar Astrophysics, NASA/Goddard Space Flight Center, Greenbelt, MD 20771, USA

Abstract

The high-magnification microlensing event MACHO-97-BLG-28 was previously determined to be a binary system composed of either two M dwarfs or an M dwarf and a brown dwarf. We present a revised light-curve model using additional data from the Mt. Stromlo 74″ telescope, model estimates of stellar limb darkening, and fitting of the blend separately for each telescope and passband. We find a lensing system with a larger mass ratio, $q = 0.28 \pm 0.01$, and smaller projected separation, $s = 0.61 \pm 0.01$, than those presented in the original study. We revise the estimate of the lens–source relative proper motion to $\mu_{\rm rel} = 2.8 \pm 0.5\,{\rm mas\,yr^{-1}}$, which indicates that 16.07 yr after the event maximum the lens and source should have separated by 46 ± 8 mas. We revise the radius of the source star using more recent reddening maps and angular diameter–color relations to $R_* = (10.3 \pm 1.9)\,R_\odot$. K- and J-band adaptive optics images of the field taken at this epoch using the NIRC2 imager on the Keck telescope show that the source and lens are still blended, consistent with our light-curve model. With no statistically significant excess flux detection we constrain the mass, $M_L = 0.24^{+0.28}_{-0.12}\,M_\odot$, and distance, $D_L = 7.0 \pm 1.0$ kpc, of the lensing system. This supports the interpretation of this event as a stellar binary in the Galactic bulge. This lens mass gives a companion mass of $M = 0.07^{+0.08}_{-0.04}\,M_\odot$, close to the boundary between being a star and a brown dwarf.

Unified Astronomy Thesaurus concepts: Exoplanets (498); Gravitational microlensing (672); Proper motions (1295)

1. Introduction

Gravitational microlensing can be used to detect exoplanets beyond the snow line (Mao & Paczyński 1991; Gould & Loeb 1992; Bennett & Rhie 1996). Unlike radial velocity and transit detection methods, microlensing does not depend on the luminosity of the host star. This means that it is possible to effectively detect planets orbiting the M-dwarfs in the Galactic bulge. Properties of microlensing systems such as the lens–source angular separation and mass ratio can be determined by modeling the observed photometric light curve. In the absence of second-order effects such as parallax or the influence of the finite size of the source (Beaulieu et al. 2006; Gaudi et al. 2008; Han et al. 2013), it is often difficult to robustly determine the physical parameters of these systems.

One way to constrain lens properties is by obtaining high angular resolution observations of the source in the years after the event. By this time the relative lens–source proper motion, typically of the order of 4–8 mas yr^{-1}, may be such that the source and lens can be resolved (Batista et al. 2015; Bennett et al. 2015). Even if they are still blended, the difference between the modeled baseline source flux and the high angular resolution measurement can be used to give an estimate of the lens brightness. These follow-up data can be obtained at large ground-based telescopes equipped with adaptive optics (AO) systems, such as Subaru (Fukui et al. 2015) and Keck (Batista et al. 2014; Beaulieu et al. 2016, 2018; Sumi et al. 2016). Even if the source and lens cannot be resolved, it may be possible to detect distortion in the point-spread function (PSF) due to the unresolved blend. This was achieved for the first time for OGLE-2012-BLG-0950Lb in Bhattacharya et al. (2018) as part

of the development of a mass-measurement method to be employed with the *WFIRST* space telescope (the *Wide Field InfraRed Survey Telescope*, Spergel et al. 2015).

In this paper we revisit the microlensing event MACHO-97-BLG-28 (Albrow et al. 1999, hereafter A1999), following the approach outlined in Batista et al. (2014, 2015) and Beaulieu et al. (2016). This event occurred prior to the first microlensing exoplanet detection, early in the history of microlensing. It was notable for being the first time that a central caustic cusp crossing was observed, and the first time limb darkening (LD) coefficients were determined by microlensing. A1999 determined the lensing system of MACHO-97-BLG-28 to be a stellar binary with mass ratio $q = 0.234$ and projected separation (in units of the Einstein ring radius, $\theta_{\rm E}$) $s = 0.686$. Two possible solutions were presented from their light-curve model: either the lens lies in the Galactic bulge and is likely to be a stellar M-dwarf binary with a separation of 1–2 au, or the lens lies closer in the Galactic disk. In this case one or both of the lens objects would be brown dwarfs. A subsequent compilation study (Alcock et al. 2000) remodeled the event and found results consistent with this interpretation.

The way that microlensing events are modeled has evolved since the event reached maximum magnification on 1997 October 18. Here we remodel this event using LD coefficients from Claret (2000), instead of deriving the coefficients from the microlensing model. The fitted LD coefficients from A1999 are in disagreement with those from Claret (2000), and this impacts on the derived source radius. Second, rather than adopting a global blend, we model the blend for each telescope and each band individually.
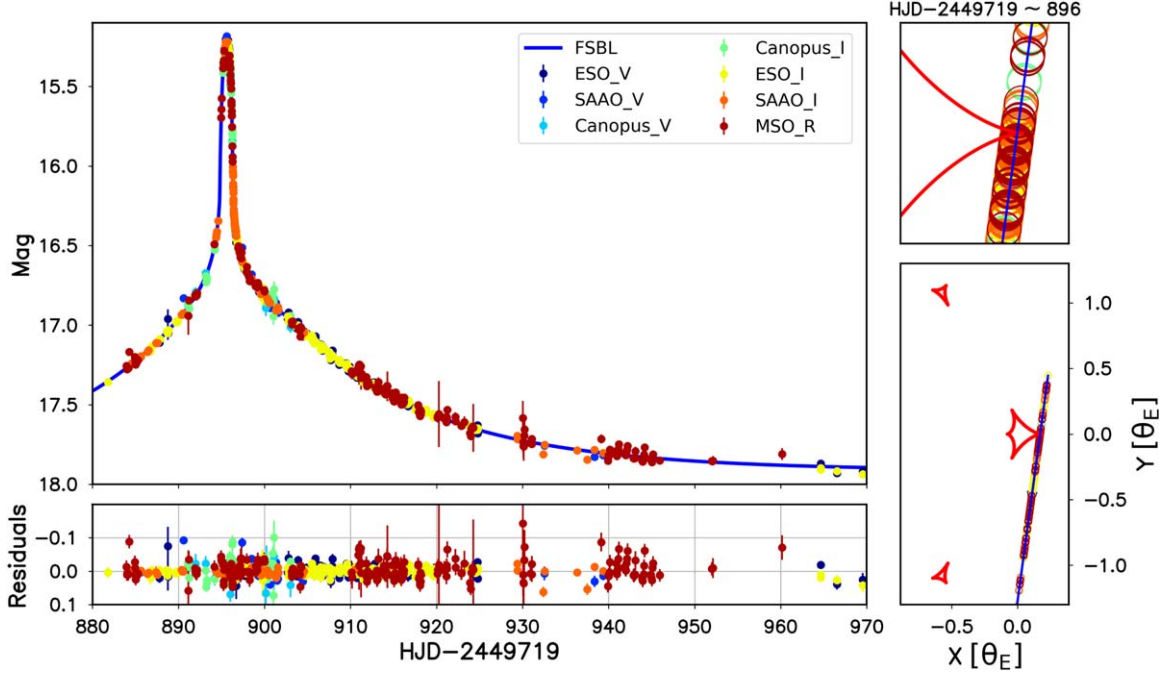
Figure 1. The light curve for MACHO-97-BLG-28 with the best-fit binary model (MOD2 rescaled). *V*-magnitudes are shown on the *y*-axis. The insert shows the caustic geometry for the MOD2 Rescaled model. The blue line indicates the source trajectory, and the size of the circles crossing the central caustic indicates the size of the source. A zoom-in on the peak for each of the four models can be found in Figure 2

We refit the light curve of MACHO-97-BLG-28 using the original data set with these modifications. We model the event using the open-source microlensing modeling package, pyLIMA (Bachelet et al. 2017), both with and without additional unpublished data from the Mt. Stromlo (MSO) 74″ telescope. Results of these models are presented in Section 2.

Finally, in an effort to obtain an accurate mass measurement of the lensing system, we observe this object with Keck AO to try to resolve the predicted bright subarcsecond blend. 16.07 yr after the event's peak, high angular resolution images were obtained of the source and blend in *J* and *K* bands in 2013 July. The relative lens–source proper motion, $\mu_{\rm rel}$, and the relative faintness of the lens compared with the source are such that both objects are still blended in the 60–80 mas seeing of our Keck images. A review of the current status of using AO observations in this manner can be found in Beaulieu (2018). The results of these Keck observations are presented in Section 3.

2. Modeling the MACHO-97-BLG-28 Light Curve with pyLIMA

The microlensing event MACHO-97-BLG-28 is located at $\alpha = 18^{\rm h}00^{\rm m}33\overset{s}{.}8$ and $\delta = -28°01'10''$ and was first observed following an alert from the Microlensing Planet Search on 1997 May 29. Dense monitoring by The Probing Lensing Anomalies NETwork collaboration followed the high-magnification increase in brightness on June 14. Observations continued for six weeks with additional baseline data points obtained in 1998 March. The full *V*- and *I*-band data set features good coverage of the event timescale, with the exceptions of the baseline pre-magnification and the sharp increase in brightness at HJD – 2449,719 = 894.8 (see Figure 1).

A1999 defined a high-quality subset of their data under the condition that $I \lesssim 14.7$ and $V \lesssim 17$ with FWHM < 2″.2. These are the data we use in our modeling. They include 431 *I*-band

images (247 from the Dutch/ESO 0.92 m at La Silla; 130 from the SAAO 1 m; and 54 from the Canopus 1 m in Tasmania) and 155 *V*-band (98 La Silla, 41 SAAO, 16 Canopus). 267 *R*-band images were also obtained by the MSO 74″. These *R*-band data cover a broad range of the event timescale and are particularly significant during the upswing toward the peak following the first caustic crossing. Unused in the original study, we augment our models with these extra data points.

2.1. Error-bar Rescaling

When modeling microlensing light curves, error bars are frequently rescaled in order to compensate for low-level systematics and general underestimation of uncertainties. Typically they are rescaled as

$$\sigma' = k\sqrt{\sigma + e_{\rm min}^2} \qquad (1)$$

where *k* is a linear scaling factor and $e_{\rm min}$ a minimum error added in quadrature. As in Bachelet et al. (2018) we avoid using the traditional metric of forcing $\chi^2/{\rm dof} = 1$ because it is is only relevant for linear models (Andrae et al. 2010). Instead we run Kolmogorov–Smirnov and Anderson–Darling residual normality tests in order to optimize error-bar scaling. These tests were applied to the ESO_I, $SAAO_I$, and MSO_R data sets only, because normality is difficult to determine for data sets with $n < 100$. Rescaling was performed when the *p*-value associated with the test was less than 1% (i.e., the test failed). With no rescaling, ESO_I passed the Kolmogorov–Smirnov test but failed the Anderson–Darling test, while for $SAAO_I$ the inverse was true. MSO_R failed both tests. We adopt $e_{\rm min} = 0.005$ for the ESO and SAAO data sets, and $e_{\rm min} = 0.01$ for the lower-precision Canopus and MSO data—a choice that is based on the quality of data obtained at these sites. The $e_{\rm min}$ term is particularly relevant to these data because there is very little coverage of the

Table 1
Uncertainty Rescaling Coefficients Used in Our Modeling

Name	N_{data}	k	e_{min}
ESO$_V$	98	1.0	0.005
SAAO$_V$	41	1.2	0.005
Canopus$_V$	16	1.2	0.01
ESO$_I$	247	1.0	0.005
SAAO$_I$	130	1.2	0.005
Canopus$_I$	54	1.2	0.01
MSO$_R$	267	1.8	0.01

baseline and it only becomes significant when the event is bright. The multiplicative k factor was introduced where e_{min} was not sufficient to make the normality tests converge, and to compensate for the underestimated error of the DAOPHOT photometry. The scaling factor for SAAO$_I$ was introduced in the other data sets with fewer data points (SAAO$_V$ and Canopus$_{V,I}$) for consistency. In the case of MSO$_R$ we adopt $k = 1.8$. A Shapiro–Wilk normality test was also performed, but no choice of scaling factors could force ESO$_I$ and MSO$_R$ to pass. The choice of rescaling parameters can be seen in Table 1.

2.2. Modeling with pyLIMA

We use the Python microlensing modeling package pyLIMA to model the event light curve. pyLIMA is the first open-source package designed specifically for microlensing (Bachelet et al. 2017), and is available on the Github platform.[6] In the first instance we perform two fits, MOD1 and MOD2, the results of which are shown in Table 2. MOD1 features the exact same high-quality subset of data used in the original study, with no rescaling. MOD2 includes the addition of the 267 MSO R-band data points. We also add two further light-curve models, MOD1 Rescaled and MOD2 Rescaled, also shown in Table 2. In these two instances the uncertainties have been scaled according to the coefficients shown in Table 1.

To speed up processing we perform these fits in two stages. First we ignore LD and constrain the grid search with a uniform-source binary lens (USBL) model using the differential evolution algorithm. Differential Evolution is a global optimizer first presented in Storn & Price (1997). Surface brightness profiles are then determined for each band (I, V, and R; Southworth 2015) by interpolating from the LD coefficients presented in Claret (2000). We base our interpolation around the spectral type of the source star determined in Section 2.3. With an intrinsic color of $(V - I)_0 = 1.07 \pm 0.15$ we estimate $T_{\mathrm{eff}} = 4600$ K and adopt $\log g = 2.85$, $\log[\mathrm{M/H}] = 0.0$, and $V_{\mathrm{micro}} = 2$ km s^{-1}. The LD coefficients that result are $u_I = 0.620$, $u_V = 0.799$, and $u_R = 0.718$. Once the most likely parameter values have been obtained from the USBL fit, we perform the more computationally intensive finite-source binary lens (FSBL) algorithm starting with these initial guesses. This reduced the FSBL computation time from 504 to 84 hr on a single-core i5-3210 m processor. Details of the FSBL method used by pyLIMA can be found in Bachelet et al. (2017). We then perform Markov Chain Monte Carlo (MCMC) explorations for all four models, utilizing the emcee algorithm (Foreman-Mackey et al. 2013) in pyLIMA.

Unlike A1999 we fit one blend parameter for each telescope and each band. This gives us a total of six blend parameters instead of two, and seven in the case of our second model. The blend parameters from the A1999 LD2 fit are given as $f_I = 0.97$ and $f_V = 0.84$. The blend parameter is defined as the ratio of the source and baseline fluxes, or the proportion of the light that is the lens. These figures indicate a small blend. In our fits we use the pyLIMA definition of the blend flux, g_i,

$$f_i(t) = f_{s,i}(A(t) + g_i); \quad g_i = \frac{f_{b,i}}{f_{s,i}} \quad (2)$$

where $A(t)$ is the magnification at time t. Compared with the small blend fractions from A1999 ($g_I = 0.031$, $g_V = 0.19$) we find ESO blends in our MOD2 fit of $g_I = 0.38 \pm 0.01$ and $g_V = 0.59 \pm 0.02$. A significant blend is to be expected for a target in the densely populated bulge. For MOD1 we minimize over 21 parameters and find $\chi^2_{\mathrm{min}} = 1650$ for 565 degrees of freedom (dof), less than A1999's preferred "LD2" model, which was arrived at with $\chi^2_{\mathrm{min}} = 1913$ over 567 degrees of freedom. For MOD2 we add the MSO data and minimize over 24 parameters. With $\chi^2_{\mathrm{min}} = 8298$ and 829 degrees of freedom, we find that the addition of the MSO data does not improve the significance of our fit. The rescaled MOD1 and MOD2, with parameters shown in Table 1, in an effort to compensate for the underestimated photometric uncertainty, show a minor increase in significance, with the addition of the MSO data resulting in the reduction of $\chi^2_{\mathrm{min}}/\mathrm{dof}$ from 1.43 to 1.37. In all models, this is a binary event with a larger mass ratio but smaller separation than A1999. Thus, though all models are similar (see also Figure 2) and result in the same physical interpretation of the system, we choose MOD2 Rescaled as our preferred model because of the minor reduction in $\chi^2_{\mathrm{min}}/\mathrm{dof}$. We hence find that the event has a mass ratio $q = 0.28 \pm 0.01$ and separation $s = 0.61 \pm 0.01$. The finite size of the source in units of Einstein Ring Radius is estimated to be 0.0251 ± 0.0003, smaller than that predicted in A1999.

2.3. Spectral Type and a New Estimate of the Radius of the Source Star

With the determination of the $(V - I)$ source color we are able to arrive at a new estimation of the size and spectral type of the source star. A1999 obtained an estimate of the size of the source star by comparing the source $(V - I)_0 - I_0$ color with that of red clump stars in the Galactic bulge, together with low-resolution spectroscopy obtained on the ESO Faint Object Spectrographic Camera on the ESO 3.6 m in Chile. Using a function from Stanek & Garnavich (1998) to describe the I-band distribution of red clump stars, and isochrones from Bertelli et al. (1994), A1999 estimated the mean radius of the source to be $R_* = (15 \pm 2) R_\odot$. Here we use the extinction calculator of the Optical Gravitational Lensing Experiment (OGLE),[7] which assumes the $E(J - K)$ measurements of Gonzalez et al. (2012), to calculate the extinction toward the source using a natural neighbor interpolation of good points. We find reddening and an I-band extinction of $E(V - I) = 1.318 \pm 0.129$ and $A_I = 1.535$. The $(V - I)$ color of the source is determined using the our calibrated baseline magnitudes from our fit in Section 2.2.
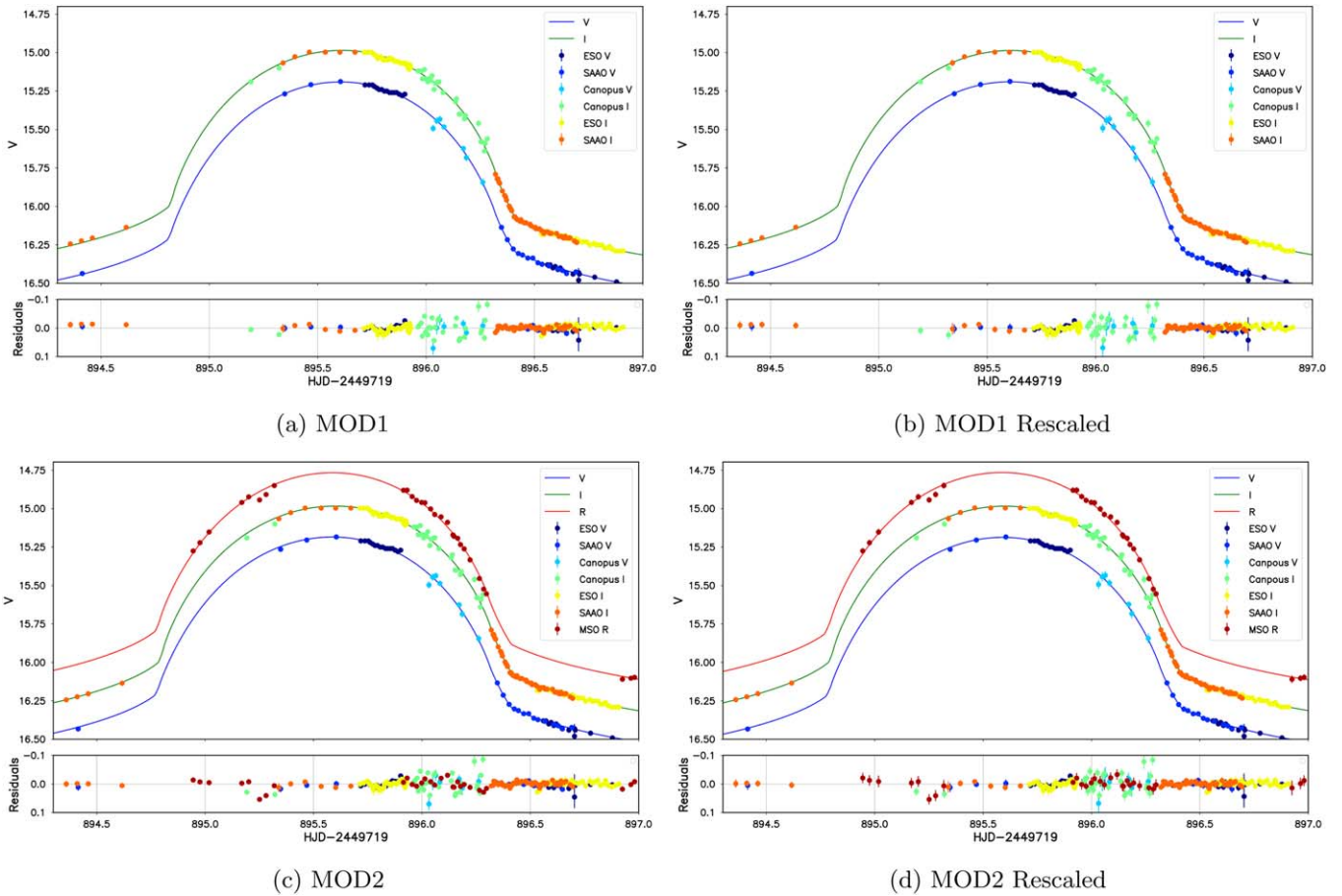
---

[6] https://github.com/ebachelet/pyLIMA

[7] http://ogle.astrouw.edu.pl/cgi-ogle/getext.py

Figure 2. Zoom-in on the event peak for all four models, with the light curves plotted for each band (*V*, *I*, and *R*). The *I* and *R* light curves have been offset by 0.2 and 0.4 magnitudes, respectively.

Table 2
Microlensing Parameters for the Microlensing Event MACHO-97-BLG-28

Parameter	MOD1	MOD1 Rescaled	MOD2	MOD2 Rescaled	A1999	A2000
t_E (days)	30.5(3)	31.0(6)	30.1(1)	30.7(5)	27.3	26.4
t_0	896.31(1)	896.30(2)	896.268(6)	896.29(2)	896.42	896.37
u_0	0.177(4)	0.171(6)	0.168(1)	0.172(5)	0.215	0.225
s	0.626(7)	0.61(1)	0.608(3)	0.61(1)	0.686	0.707
q	0.254(6)	0.27(1)	0.288(3)	0.28(1)	0.234	0.210
α (rad)	−1.702(2)	−1.705(3)	−1.709(1)	−1.705(3)	−1.712	−1.705
ρ_* (10^{-3})	0.0248(3)	0.0245(5)	0.0257(1)	0.0251(3)	0.0286	0.0288(5)
DOF	565	565	829	829	567	1404
χ^2_{min}	1650	812	8298	1135	1913	2734.9

Note. Presented here are four FSBL fits for the MACHO-97-BLG-28 light curve, with the LD2 fit parameters from A1999 presented for comparison. These fits were achieved by performing a global optimization with the Differential Evolution algorithm in pyLIMA, followed by Markov Chain explorations. The number in brackets notes the 68% error in the last digit derived from the MCMC. MOD1 uses the same data set as A1999. MOD2 includes an extra 267 *R*-band data points from the MSO 74″. MOD1 Rescaled and MOD2 Rescaled are the fits when the data are rescaled as per Table 1 and Section 2.1. We define u_0 according to the center of mass of the system, contrary to A1999, which defined it as centered on the binary midpoint (see Appendix A of Albrow et al. 2000). The A1999 values above have been converted to the center-of-mass parameterization.

With calibrated (and deblended) source baseline magnitudes of $V = 18.45 \pm 0.05$ and $I = 16.06 \pm 0.05$ we find $(V - I) = 2.39 \pm 0.07$. After correction for extinction we estimate the intrinsic color to be $(V - I)_0 = 1.07 \pm 0.15$. Using Bessell & Brett (1988) and Bessell (1990), we revise the estimate of the source from a K2 giant to a K0/K1 giant. We refer to the angular diameter–color relations presented in Adams et al. (2018), which extend the relations presented in Boyajian et al.

(2013, 2014) by using a sample of dwarfs/subgiants and a sample of giant stars. We use the coefficients

$$\log(2\theta_*(\mathrm{mas})) = (0.535 \pm 0.027) + (0.490 \pm 0.046)(V - I) \\ - (0.068 \pm 0.019)(V - I)^2 - 0.2I \quad (3)$$

in order to determine the angular size of the source. These, combined with the extinction law from Gonzalez et al. (2012)

and Nishiyama et al. (2009), give an angular radius $\theta_* = 6.0 \pm 1.1\,\mu$as and a radius of $R_* = (10.3 \pm 1.9)\,R_\odot$, which is notably smaller than that predicted in A1999. Our determination of the angular radius of the source, however, is in good agreement with that determined in Alcock et al. (2000), $\theta_* = 6.58 \pm 0.90\,\mu$as.

2.4. Angular Size of the Einstein Ring

When modeling this event our data were calibrated with the same SAAO calibration as A1999. As in A1999 this results in a modeled baseline source+blend flux of $I = 15.66 \pm 0.05$ and $V = 17.95 \pm 0.05$. With an ESO_V blend factor of 0.59 ± 0.02 and ESO_I blend factor of 0.38 ± 0.01 (with the blend factor in PyLIMA defined as the ratio of the blend and source fluxes) we find a deblended source magnitude of

$$V_s = 18.45 \pm 0.05$$
$$I_s = 16.06 \pm 0.05. \qquad (4)$$

Data coverage over the caustic crossing (see the top right panel in Figure 1) indicates the presence of finite-source effects, which means that we are able to determine the crossing time (t_*) for the radius of the source and estimate the relative source–lens proper motion. Combining our calculation of the radius of the source star from Section 2.3 with our modeled finite size of the source, ρ_*, we can calculate the angular Einstein ring radius,

$$\theta_E = \theta_*/\rho. \qquad (5)$$

We find an angular Einstein ring radius of $\theta_E = 0.24 \pm 0.04$ mas and a lens–source relative proper motion of $\mu_{\rm rel} = 2.8 \pm 0.5\,{\rm mas\,yr^{-1}}$, the latter of which is smaller than the A1999 estimate of $\mu_{\rm rel} = 4.09 \pm 0.55\,{\rm mas\,yr^{-1}}$. With the 16.07 yr between observations we hence calculate the predicted lens–source separation at the time of our follow-up observations to be 46 ± 8 mas, which is of the order of the best FWHM photometry achievable from Keck.

3. AO Observations of MACHO-97-BLG-28

MACHO-97-BLG-28 was observed using the NIRC2 AO Imager with the Keck II telescope on Maunakea on 2013 July 13 (HJD = 2456487.291), with the intent of resolving the source and lens—or finding PSF distortions as in Bhattacharya et al. (2018)—and hence being able to constrain the lens mass–distance relation. We use the narrow camera, which results in a plate scale of 0.01 arcsecond pixel^{-1}. Ten images were obtained in J and K, each with an exposure time of 10 s and a dither of $0\farcs7$. Our images feature a median FWHM of 64 mas in K and 78 mas in J, which, while greater than the predicted lens–source separation, still facilitates a measurement of the excess flux. We reduce these data following the procedure described in Beaulieu et al. (2016) and Batista et al. (2014), beginning with standard dark current and flat-field corrections. We align a single Keck image with data from the VVV Survey (Minniti et al. 2010). As the precision of the dithering is greater than that of the pointing, astrometry was performed manually on the remaining images with the first used as a reference. A catalog of sources was generated from this reference image using SExtractor (Bertin & Arnouts 1996), with it being used to realign each image in turn. The data were then stacked
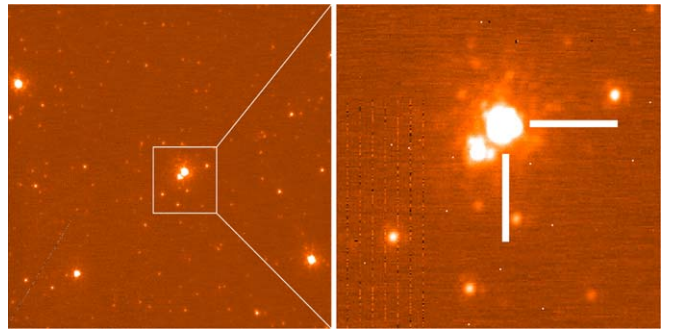

Figure 3. Keck II K-band images of the source star field of the microlensing event MACHO-97-BLG-28, taken with the narrow camera on NIRC2. The left image is the full 10 arcsecond Keck frame. The right image is a 2 arcsecond zoom centered on the source star.
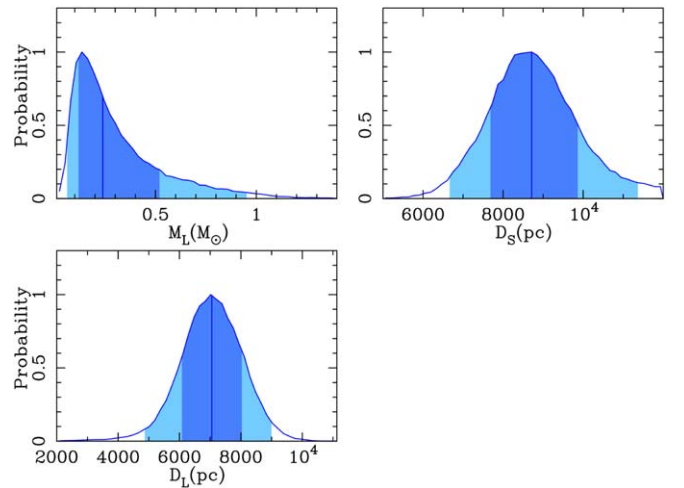

Figure 4. Posterior probability distributions of the physical properties of the system determined using a Galactic model (Sumi et al. 2011). The inner dark regions represent the 1σ limits while the light blue regions represent 2σ. Shown are M_L, the lens mass, D_L, the lens distance, and D_S, the distance to the source.

using SWARP (Bertin 2010) and the calibration constant calculated by cross-matching the K images with the VVV catalog. This process was repeated for the data in the J band. The final stacked K-band image can be seen in Figure 3. We find K- and J-band magnitudes at the predicted position of the source to be

$$(J, K)_{\rm Keck} = (14.12, 12.92) \pm (0.07, 0.06). \qquad (6)$$

These magnitudes were calculated by comparing our photometry with the VVV magnitudes at the source position: $J_{\rm VVV} = 13.92 \pm 0.02$ and $K_{\rm VVV} = 12.76 \pm 0.02$.

To determine whether there is an excess flux detection, we compare this Keck measurement with the predicted K and J baseline magnitudes derived from our modeled unmagnified source flux, $(V, I)_{s,\rm model} = (18.45, 16.06) \pm (0.05, 0.06)$. We perform a Monte Carlo simulation with $(V, I)_{b,\rm model}$, A_V, A_I, A_J, and A_K as parameters. Estimated distance modulus, age, and metallicity are derived from isochrone models (Bressan et al. 2012) as in Bennett et al. (2018). We use isochrone models with $-0.3 < [{\rm M/H}] < 0.3$ and $10\,{\rm Gyr} < {\rm age} < 13\,{\rm Gyr}$, approximating the bulge, to derive J and K. We find the (predicted) unmagnified source
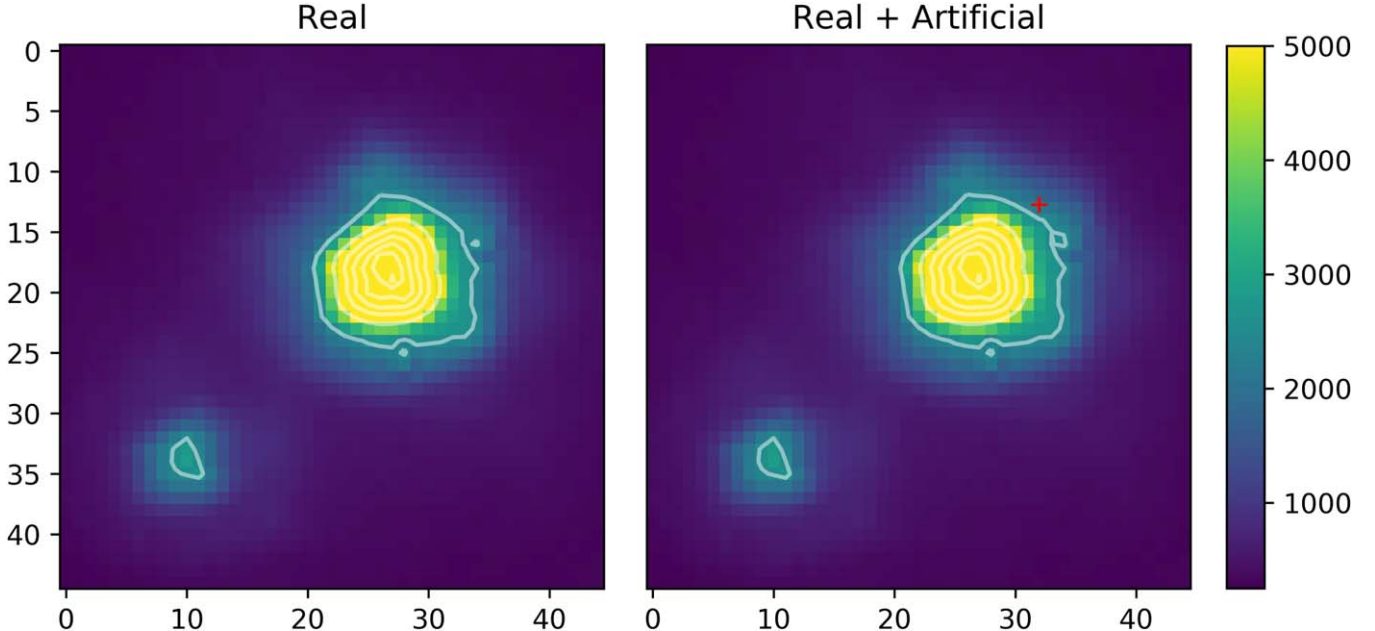
Figure 5. Comparison of the Keck K-band images combined with SWARP (left), and the same image augmented with an artificial lens star at 63 mas separation (right), generated by DAOPHOT. The axes in both images are in pixels, where each pixel represents $0\rlap{.}''01$. The color gradient represents the number of pixel counts. The position of the centroid of the artificial star is marked with a red cross. The separation and magnitude contrast are such that the source and lens could not be resolved if further AO observations of this event were made in 2019.

magnitudes to be

$$J = 14.18^{+0.20}_{-0.17}$$
$$K = 13.04^{+0.27}_{-0.22}. \qquad (7)$$

The large errors in these values are dominated by the uncertainty in metallicity and age. Comparing the measured source magnitudes in (6) with those predicted in (7), we find no statistically significant excess flux detection.

3.1. Physical Parameters and Contemporary Observations

To determine the physical parameters of the system we perform a Bayesian analysis using the Galactic model from Sumi et al. (2011). Posterior distributions of the source distance, D_S, lens mass, M_L, and lens distance, D_L, are presented in Figure 4. In this calculation we consider the mass ratio and separation as priors, and ignore the case where the lens is a remnant. With no excess flux detection, we weakly constrain the lens mass, $M_L = 0.24^{+0.28}_{-0.12}\,M_\odot$, and lens distance, $D_L = 7.0 \pm 1.0$ kpc. With our preferred MOD2 Rescaled mass ratio of $q = 0.28 \pm 0.01$, this slightly favors the conclusion that the event is a stellar M-dwarf binary, though the other option proposed in A1999 of an M dwarf and brown dwarf cannot be ruled out.

To determine whether or not further AO observations might be worthwhile in 2019, we generate an artificial star on one of our K-band images using the ADDSTAR routine from DAOPHOT (Stetson 1987). This star is placed 63 mas from the centroid of the source—the projected separation of the source and lens were that object to be observed in 2019. On inspection of the contour-plot images, seen in Figure 5, we find no significant difference between the real 2013 K-band image and the synthetic one. We conclude that the separation and magnitude contrast are such that the source and lens could

not be resolved if further AO observations of this event were made in 2019.

4. Discussion and Conclusion

In this study we revisit the microlensing event MACHO 97-BLG-28 and confirm the interpretation of A1999 that it is a stellar binary. Following Figure 4 we estimate a companion mass of $M = 0.07^{+0.08}_{-0.04}\,M_\odot$, right on the boundary between being a star and a brown dwarf. We use the open-source microlensing code being developed for the next generation of microlensing studies, pyLIMA, and unused R-band data from Mt. Stromlo, to improve the robustness of the light-curve model. We adopt LD parameters from stellar profile estimates determined subsequent to the original study and, as is standard in contemporary microlensing practice, fit blend parameters for each band and each telescope. Our refined parameters of this event find it to be a stellar binary with mass ratio $q = 0.28 \pm 0.01$, projected separation $s = 0.61 \pm 0.01$, and characteristic timescale $t_E = 30.7 \pm 5$ days, which is $\sim$12.5% longer than that predicted previously. Consistency is seen between different models, with only a modest improvement in $\chi^2_{\min}/\mathrm{DOF}$ from 1.43 to 1.37 following the introduction of the MSO$_R$ data. These new models, however, are shifted consistently from the A1999 model.

This study is the first attempt to observe a stellar binary microlensing event with high-resolution AO. It is also the first attempt to observe high-resolution follow-up of an event with a giant source star. Even though there was no statistically significant lens detection, the technique as presented here (a) can be used on events with sufficient lens–source separation and proper motion that the source and lens can be resolved, and (b) will be used in future with the next generation of telescopes such as the Extremely Large Telescope, Giant Magellan Telescope, and Thirty Meter Telescope, which will have three times the resolution of Keck and hence be able to resolve them sooner. Further, this

ORCID iDs

J. W. Blackman https://orcid.org/0000-0001-5860-1157
J.-P. Beaulieu https://orcid.org/0000-0003-0014-3354
A. A. Cole https://orcid.org/0000-0003-0303-3855
A. Vandorou https://orcid.org/0000-0002-9881-4760
N. Koshimoto https://orcid.org/0000-0003-2302-9562
E. Bachelet https://orcid.org/0000-0002-6578-5078
D. P. Bennett https://orcid.org/0000-0001-8043-8413

References

Adams, A. D., Boyajian, T. S., & von Braun, K. 2018, MNRAS, 473, 3608
Albrow, M. D., Beaulieu, J.-P., Caldwell, J. A. R., et al. 1999, ApJ, 522, 1011
Albrow, M. D., Beaulieu, J. P., Caldwell, J. A. R., et al. 2000, ApJ, 534, 894
Alcock, C., Allsman, R. A., Alves, D. R., et al. 2000, ApJ, 542, 281
Andrae, R., Schulze-Hartung, T., & Melchior, P. 2010, arXiv:1012.3754
Bachelet, E., Bozza, V., Han, C., et al. 2018, ApJ, 870, 11
Bachelet, E., Norbury, M., Bozza, V., & Street, R. 2017, ApJ, 154, 203
Batista, V., Beaulieu, J.-P., Bennett, D. P., et al. 2015, ApJ, 808, 170
Batista, V., Beaulieu, J. P., Gould, A., et al. 2014, ApJ, 780, 54
Beaulieu, J.-P. 2018, Univ, 4, 61
Beaulieu, J.-P., Batista, V., Bennett, D. P., et al. 2018, AJ, 155, 78
Beaulieu, J.-P., Bennett, D. P., Batista, V., et al. 2016, ApJ, 824, 83
Beaulieu, J.-P., Bennett, D. P., Fouqué, P., et al. 2006, Natur, 439, 437
Bennett, D. P., Bhattacharya, A., Anderson, J., et al. 2015, ApJ, 808, 169
Bennett, D. P., & Rhie, S. H. 1996, ApJ, 472, 660
Bennett, D. P., Udalski, A., Bond, I. A., et al. 2018, ApJ, 156, 113
Bertelli, G., Bressan, A., Chiosi, C., Fagotto, F., & Nasi, E. 1994, A&AS, 106, 275
Bertin, E. 2010, SWarp: Resampling and Co-adding FITS Images Together, V2.38.0, Astrophysics Source Code Library, ascl:1010.068
Bertin, E., & Arnouts, S. 1996, A&AS, 393, 117
Bessell, M. S. 1990, PASP, 102, 1181
Bessell, M. S., & Brett, J. M. 1988, PASP, 100, 1134
Bhattacharya, A., Beaulieu, J.-P., Bennett, D. P., et al. 2018, ApJ, 156, 289
Boyajian, T. S., Von Braun, K., Van Belle, G., et al. 2013, ApJ, 771, 40
Boyajian, T. S., von Braun, K., van Belle, G., et al. 2014, ApJ, 787, 92
Bressan, A., Marigo, P., Girardi, L., et al. 2012, MNRAS, 427, 127
Claret, A. 2000, A&A, 363, 1081
Foreman-Mackey, D., Hogg, D. W., Lang, D., & Goodman, J. 2013, PASP, 125, 306
Fukui, A., Gould, A., Sumi, T., et al. 2015, ApJ, 809, 74
Gaudi, B. S., Bennett, D. P., Udalski, A., et al. 2008, Sci, 319, 927
Gonzalez, O. A., Rejkuba, M., Zoccali, M., et al. 2012, A&A, 543, A13
Gould, A., & Loeb, A. 1992, ApJ, 396, 104
Han, C., Udalski, A., Choi, J.-Y., et al. 2013, ApJL, 762, L28
Mao, S., & Paczyński, B. 1991, ApJL, 374, L37
Meyer, M. R., Amara, A., Reggiani, M., & Quanz, S. P. 2018, A&A, 612, L3
Minniti, D., Lucas, P. W., Emerson, J. P., et al. 2010, NewA, 15, 433
Nishiyama, S., Tamura, M., Hatano, H., et al. 2009, ApJ, 696, 1407
Southworth, J. 2015, JKTLD: Limb darkening coefficients v3, Astrophysics Source Code Library, ascl:1511.016
Spergel, D., Gehrels, N., Baltay, C., et al. 2015, arXiv:1503.03757
Stanek, K. Z., & Garnavich, P. M. 1998, ApJ, 503, 131
Stetson, P. B. 1987, PASP, 99, 191
Storn, R., & Price, K. 1997, Journal of Global Optimization, 11, 341
Sumi, T., Kamiya, K., Bennett, D. P., et al. 2011, Natur, 473, 349
Sumi, T., Udalski, A., Bennett, D. P., et al. 2016, ApJ, 825, 112